# Plasma density gradients at the edge of polar ionospheric holes: The absence of phase scintillation

Luke A. Jenner, [1], Alan G. Wood [1], Gareth D. Dorrian [1], Kjellmar Oksavik [2, 3], Timothy K. Yeoman [4], Alexandra R. Fogg [4], and Anthea J. Coster [5]

[1] School of Science & Technology, Nottingham Trent University, Nottingham, UK.
[2] Birkeland Centre for Space Science, Department of Physics and Technology, University of Bergen, Bergen, Norway
[3] Arctic Geophysics, University Centre in Svalbard, Longyearbyen, Norway
[4] Department of Physics and Astronomy, University of Leicester, Leicester, UK.
[5] MIT Haystack Observatory, Massachusetts, USA.

*Correspondence to*: Alan G. Wood (alan.wook@ntu.ac.uk)

**Abstract.** Polar holes were observed in the high-latitude ionosphere during a series of multi-instrument case studies close to the northern hemisphere winter solstice in 2014 and 2015. These holes were observed during geomagnetically quiet conditions and under a range of solar activities using the European Incoherent Scatter Scientific Association (EISCAT) Svalbard Radar (ESR) and measurements from Global Navigational Satellite System (GNSS) receivers. Steep electron density gradients have been associated with phase scintillation in previous studies, however, no enhanced scintillation was detected within the electron density gradients at these boundaries. It is suggested that the lack of phase scintillation may be due to low plasma density levels and a lack of intense particle precipitation. It is concluded that both significant electron density gradients and that plasma density levels above a certain threshold are required for scintillation to occur.

## 1 Introduction

The F-region ionosphere is a weakly ionised plasma in the Earth's atmosphere extending from an altitude of ~150 to ~500 km, above which it merges with Earth's plasmasphere. Large-scale plasma structures with a horizontal extent of tens to hundreds of km are routinely observed in the F-region high-latitude ionosphere (Tsunoda, 1988). One type of structure commonly observed are polar cap patches, also referred to as patches, which are enhancements of plasma density with at least twice the background value and have a horizontal spatial extent of 100 km or greater (Crowley, 1996). Buchau et al. (1983) observed such patches of enhanced ionisation drifting antisunward with the background plasma flow in the central region of the polar cap at Thule, Greenland (77.5° N, 69.2° W; 85.4° MLAT, 32.4° MLON). The patch densities were larger than could be produced due to the observed flux of precipitating particles, and it was concluded that the patches were not produced locally by precipitation. Weber et al. (1984) suggested that the patches were produced on the dayside at auroral or subauroral latitudes and then convected antisunward to higher, polar latitudes. A comparison of average maps of the electron density and high-latitude convection pattern suggested that solar-produced plasma was drawn into the polar cap as a continuous density enhancement known as the Tongue-of-Ionisation (TOI) (Foster et al., 1984). Several mechanisms have been proposed to break

a TOI into a series of patches, including variations in the high-latitude convection pattern moving flux tubes in and out of sunlight (Anderson et al., 1988), expansion and contraction of the high-latitude convection pattern in response to transient bursts of reconnection drawing in plasma from different latitudes (Cowley and Lockwood, 1992; Lockwood and Carlson, 1992; Carlson et al., 2002, 2004, 2006), variations in the y-component of the Interplanetary Magnetic Field (IMF) drawing in plasma from different magnetic local times (MLT) (Sojka et al., 1993), variation of the z-component of the IMF altering whether plasma could be drawn in to the polar cap (Valladares et al., 1998), erosion of plasma densities due to enhanced recombination during a flow channel event (Rodger et al., 1994; Valladares et al., 1994), and modification of the density of the photoionised plasma transported into the polar cap by particle precipitation (Walker et al., 1999; Millward et al., 1999). Patches have been observed travelling thousands of kilometres across the polar regions (Weber, 1986; Oksavik et al., 2010; Nishimura et al., 2014), and are primarily associated with times when the z-component of the IMF is negative (Buchau and Reinisch, 1991).

Blobs are also plasma density enhancements, however, unlike patches, they occur outside the polar cap. They are further categorised into boundary blobs, subauroral blobs, and auroral blobs (Rino, 1983; Jin et al., 2016). Boundary blobs are found near the equatorward auroral boundary, neighbouring the ionospheric trough's poleward wall. Parkinson et al. (2002) observed patches leaving the polar cap, slowing in the antisunward direction and then beginning to move zonally. It was suggested that these patches would form boundary blobs, and this was later confirmed by Pryse et al. (2006) who compared the plasma density in a polar cap patch to that within a boundary blob which the patch subsequently formed. Subauroral blobs have a similar appearance to boundary blobs, however, they are found in the ionospheric trough. Auroral blobs are found within the auroral oval and seem to be longitudinally restricted. The most likely mechanism for their creation is particle precipitation (Jones et al., 1997).

Not all ionospheric structures are enhancements of the background plasma; polar ionospheric holes are regions of low plasma density. Brinton et al. (1978) observed a depletion of this kind under conditions of low solar activity (F10.7=71 sfu) and low magnetic activity ($K_p = 2$). This depletion was also associated with a minimum of electron temperatures, indicating the absence of local particle precipitation. Polar holes are generally located between 21 and 06 MLT and 70°-80° magnetic latitude and typically have steep plasma density gradients at their boundaries. They are believed to be produced when plasma in the high-latitude convection pattern circulates in perpetual darkness. Plasma loss by recombination in the absence of a plasma source causes density levels to drop. This idea is supported by the conditions under which polar holes have generally been observed, namely quiet geomagnetic activity ($K_p$ 2 or less) when the contribution to the plasma densities from particle precipitation will be low (Brinton et al., 1978). The electron densities inside of the polar holes are seen to reach a minimum in the range of $10^8$-$10^{11}$ electrons·m$^{-3}$ (Obara and Oya, 1989, Benson and Grebowsky, 2001) and, while there is variation between holes, inside of a singular polar hole the density level is very consistent.

Smaller scale structures can arise at steep plasma density gradients due to instability processes such as the gradient-drift instability (GDI) (Keskinen and Ossakow, 1983) and the velocity shear driven instability (Kelvin-Helmholtz instability, KHI). Carlson et al. (2008) proposed and that the real process involves both mechanisms acting on different time scales. The smaller scale (tens of meters to tens of kilometers) plasma density structures that arise cause variations in the refractive index of the ionosphere. As a GNSS signal passes through this region, refraction and/or diffraction of the radio wave causes fluctuations in the phase and amplitude of the signal. Ionospheric scintillation is the rapid fluctuation of the received signal which can disrupt applications using GNSS, as thoroughly reviewed by Hapgood (2017). Since the second world war, large numbers of studies have shown the effect of ionospheric irregularities on radio signals, as reviewed by Aarons (1982). The morphology of these irregularities has been extensively studied at high-latitudes (e.g. Kersley, 1972), together with the effects upon the propagation of radio signals in this region (e.g. Kersley et al., 1995).

More recently studies have focussed on Global Navigation Satellite System (GNSS) frequencies, where scintillation poses a substantial threat to the integrity, availability and accuracy of GNSS positioning, leading to positioning errors and service outages due to signal tracking problems at the GNSS receiver. A direct connection between gradients in the Total Electron Content (TEC) at the edge of a plasma stream with both phase and amplitude scintillation has been observed (Mitchell et al., 2005) and plasma structuring caused by auroral precipitation has been linked to the loss of signal lock by a GNSS receiver (Elmas et al., 2011; Smith et al., 2008; Oksavik et al., 2015). A statistical study has shown an agreement between both phase and amplitude scintillation with the asymmetric distribution of polar cap patches around magnetic midnight (Spogli et al., 2009) and that auroral emissions correlate with GNSS signal phase scintillation (Kinrade et al., 2013; van der Meeren et al., 2015). Phase and amplitude scintillation can be associated with the larger spatial structures associated with polar cap patches (Alfonsi et al., 2011). The climatology of ionospheric scintillation at polar latitudes in the northern hemisphere was determined over almost two solar cycles, and the dependence upon solar cycle, geomagnetic activity and solar wind conditions was shown by De Franchesci et al. (2019). Phase scintillation is usually the dominant process at high latitudes (Spogli et al., 2009; Prikryl et al., 2015) and this is the focus of the present study.

Phase scintillation is commonly quantified by the standard deviation of the signal phase, $\sigma_\varphi$, which is usually computed across 60 seconds. The refractive component of the signal is usually assumed to be slowly varying and associated with frequencies of less than 0.1 Hz. Therefore, by only considering frequencies greater that 0.1 Hz, the diffractive effects (usually referred to as scintillation) can be distinguished (Fremouw et al., 1978). However, the 0.1 Hz cutoff can give spurious observations of phase scintillation as a result of erroneous data detrending (Forte and Radicella, 2002). When a GNSS satellite is observed at low elevation angles the $\sigma_\varphi$ index cannot distinguish between phase scintillation and background noise for weak to moderate phase scintillation (Forte, 2005). Wang et al. (2018) showed that rapid variations in the phase of a trans-ionospheric signal can arise as a result of plasma structures moving rapidly relative to an observer at ground level, and so can give the appearance of phase scintillation. Rapid changes in the spatial distribution of electron density can also introduce similar effects as the

GNSS satellite-to-receiver ray path can sweep through these irregularities at high speed, resulting in high-frequency refractive variations (McCaffrey and Jayachandran, 2019).

The presence or absence of scintillation effects on trans-ionospheric radio signals have been extensively studied for electron density enhancements in the high-latitude ionosphere, but the effect of the steep plasma density gradients at the edge of depletions, such as polar holes are not as extensively studied. The purpose of this paper is to report on the effects of such steep density gradients on GNSS signals, observed in three multi-instrument case studies close to northern winter solstice, and to provide observational evidence which supports the work of Aarons (1982).

## 2 Instrumentation

The European Incoherent Scatter Scientific Association (EISCAT) operates the EISCAT Svalbard Radar (ESR) at Longyearbyen (78.2° N, 16.0° E; 15.2° MLAT, 112.9° MLON) on Svalbard (Wannberg et al., 1997). The site consists of two antennas, a 32-meter parabolic dish and a 42-meter parabolic dish. The 42 m dish is fixed along the direction of the local geomagnetic field lines (azimuth -179°; elevation 81.6°), while the 32 m dish is steerable in both azimuth and elevation. Observations of the electron density, electron temperature, ion temperature, and ion drift line of sight velocity in the ionosphere from this incoherent scatter radar (ISR) are used in this study.

The Super Dual Auroral Radar Network (SuperDARN) is a network of high latitude coherent scatter radars (Greenwald et al., 1995; Chisham et al., 2007; Nishitani et al,. 2019) that observe line-of-sight plasma velocities in the F-region. These measurements are assimilated using the map potential technique (Ruohoniemi and Baker, 1998), which uses an ionospheric convection model to map the electrostatic potential pattern. Electrostatic equipotential lines are streamlines of ionospheric convection flows. As the plasma drift velocity is perpendicular to both the electric and magnetic fields in the F-region ($\underline{E}\times\underline{B}$ drift) the plasma convection pattern can be directly inferred from the electric potential maps.

GNSS signals detected by NovAtel GPStation-6 receivers at the Kjell Henriksen Observatory (KHO) (78.2° N, 16.0° E; 15.2° MLAT, 112.9° MLON ) can be used to infer the effects of the ionosphere on radio waves traveling though this medium. Amplitude scintillation is measured using the $S_4$ index, which is the square root of the variance of received power divided by the mean value of the received power (Briggs and Parkin, 1963). Phase scintillation is measured using the $\sigma_\phi$ index, which is the standard deviation of the detrended carrier phase $\phi$ in radians (Fremouw et al., 1978) over 60 seconds.

The IMF was observed by the Advanced Composition Explorer (ACE), which is a NASA Spacecraft orbiting the L1 Lagrangian point of the Earth Sun system, roughly 1.54 million km from the Earth (Zwickl et al., 1998). In addition to the x-, y- and z- components of the IMF the clock angle, given by $arctan\frac{|B_y|}{|B_z|}$, is also considered. When the clock angle is greater

than 45 degrees either $|B_y|>|B_z|$ or $B_z<0$, in either case a two cell convection pattern is expected with antisunward flow drawing plasma from day to night across the polar cap (Thomas and Shepherd, 2018).

125 Total Electron Content (TEC) maps are used to put these measurements into context. These were obtained from the Madrigal Database at the MIT Haystack Observatory (Ridout and Coster, 2006; Vierinen et al., 2015). Two other indices are used within this study. The $K_p$ index is used as a proxy for disturbances to the geomagnetic field. The F10.7 cm solar flux is used as a proxy for solar activity. These indices were both obtained from the UK Solar System Data Centre (UKSSDC) at Rutherford Appleton Laboratory, UK.

## 3 Results

### 3.1 Case study: 17th December 2014

The 3-hourly $K_p$ values observed on 17th December 2014 between 12:00 and 23:59 UT ranged between 1- and 1+, indicating quiet conditions. The F10.7 cm solar flux was relatively high, the value of 198.5 sfu is typical of solar maximum. The IMF observed by the ACE spacecraft between 12:00 and 23:59 UT (Fig. 1) was characterised by a positive value for the IMF $B_y$

135 (mean value 3.9 nT). IMF $B_z$ was more variable, but generally took smaller values (mean value of 1.7 nT). The clock angle was generally greater than 45° from 14 UT until 19 UT, and the corresponding SuperDARN plots (discussed later in this section) show that a two cell convection pattern dominated until at least 20 UT.

Total Electron Content (TEC) maps (Fig. 2) show the overall plasma density throughout the high-latitude regions. The TEC maps at 12 UT and 15 UT show values of ~2 TECu (dark blue colour) in the polar cap. At 18 UT at 21 UT larger electron

140 densities can be observed crossing the polar cap in a two cell convection pattern, with values of ~15 TECu (yellow colour), indicating that plasma produced by photoionisation on the dayside is being drawn into the polar cap. This plasma is being drawn into the polar cap during relatively quiet conditions ($K_p$~1) and is consistent with a two cell convection pattern.

The electron densities and temperatures observed by the field-aligned 42 m dish of the EISCAT Svalbard Radar (ESR) between 12:00 UT and 23:59 UT are shown in Fig. 3. The scales on this plot have been chosen to enable a clear comparison

145 with other figures presented in this paper. A clear depletion in the electron densities is observed between approximately 16 and 18 UT at all altitudes. The electron and ion temperatures are not elevated at this time with values of approximately 1000 K, suggesting that this depletion is void of particle precipitation and did not arise from enhanced recombination due to Joule heating. The ESR does not show a substantial plasma velocity aligned with the radar beam. This radar observed at an elevation of 81.6° which is aligned with the magnetic field line in the F-region. There was no substantial component of velocity observed

150 along the magnetic field line. In order to further investigate the electron density depletion, a line plot of the maximum detected electron density from 90-400 km is shown (Fig. 4). In addition to the maximum density two other values are present on the plot, the average value for the whole day, and 35% of the average value. The depletion was defined as when the electron

density dropped below the 35% line and, in this case, the depletion was defined as starting at 16:29 UT and ending at 18:00 UT.

155    Fig. 5 shows the high-latitude convection pattern inferred from the SuperDARN radars for three representative times during the time that the electron density depletion was observed by the ESR. These clearly show a two cell convection pattern, with plasma drawn antisunward across the polar cap. The ESR observes at a given location, which rotates under the convection pattern. The depletion, identified in Fig. 4, is indicated by a black line. At midwinter Svalbard is in perpetual darkness. On $14^{th}$ December the ground level terminator is at a maximum latitude of 68° N, which corresponds to a maximum magnetic
160    latitude of 76° MLAT at 21 UT. This depletion is nightward of the terminator and the SuperDARN convection patterns suggest that this plasma is circulating in perpetual darkness. It is interpreted as a polar hole.

The data collected by the GNSS receiver was from the GPS, Galileo and GLONASS systems and the receiver provides the azimuth and elevation of the satellite with respect to the receiver. This was converted into a latitude and longitude using the radio wave path and assuming that the data corresponds to 350 km in altitude, in line with previous studies (e.g. Cervera and
165    Thomas, 2006; Forte and Radicella, 2002). At low elevation angles the GNSS TEC and scintillation data can become unreliable due to multi-path issues, so observations at an elevation of less than 30° were discarded. This cut of has been used in previous studies, for example Mitchell et al. (2005). Signal lock times below 240 seconds were also discarded, in line with previous studies (e.g. van der Meeren et al., 2015). The satellite tracks were overlaid onto SuperDARN plots. (Fig. 5)

TEC and phase scintillation data from GNSS receivers were taken during times when the polar hole was observed. This hole
170    is observed for 1.5 hours and several satellite paths are present during this time window. The GNSS TEC data clearly show lower TEC levels at and around the area marked by the ESR as a hole and, on some of the satellite trajectories, sharp changes can be seen with the edge of the hole. A one-to-one correspondence between the GNSS TEC data and the EISCAT data is neither expected or observed. It is highly likely that the polar hole will evolve during the time for which it is observed, and therefore the plots in figure 5 include both spatial and temporal variation. The ESR observes the polar hole for 91 minutes and
175    the plasma velocity inferred from the electric potential patterns inferred from the SuperDARN radars (figure 5) at this location is of the order of 150 m s$^{-1}$, indicating that the polar hole has a horizontal extent of some 800 km in a direction parallel to the plasma flow. In summary the combination of the EISCAT and GNSS TEC measurements indicate that the polar hole is present for an extended period of time (of the order of hours) over a large (hundreds of km) spatial scale.

Panels showing the location of phase scintillation on the satellite tracks are also shown in figure 5. A threshold of 0.2 rad was
180    used to identify phase scintillation. Different authors have used different thresholds for phase scintillation, including 0.2 rad (e.g. van der Meeren, 2015), 0.25 rad (e.g. Alfonsi et al., 2011) and 0.3 rad (e.g. Kinrade et al., 2013). The purpose of using a low threshold within the present study was to ensure that any possible indication of phase scintillation was included. Since

TEC and scintillation are collected simultaneously, comparing the two might be expected to show increased scintillation where there are changes in TEC. No scintillation was observed on the edges of the holes.

## 3.2 Case study 2: 10th December 2015

The F10.7cm solar flux for this case was lower than in the first study, with a value of 108.5 sfu. The $K_p$ index was higher, with a value of 3 from 12 to 18 UT and a value of 4 at 21 and 24 UT, indicating an active state, but not storm levels. Once again the IMF was variable, with $B_z$ taking positive and negative values. $B_y$ was consistently larger than $B_z$ and dominated. As in the previous case study a two cell convection pattern was observed.

The TEC maps at 18 and 21 UT are shown in Fig. 7. As in the previous case study these indicate higher density plasma produced at lower latitudes being drawn across the polar cap within the high latitude convection pattern, with this effect maximising at 21 UT.

The 42 m ESR observations (Fig. 8) for this day show an electron density depletion that contains all the previously discussed markers, with no significant velocity in the field aligned direction.

Using the same method as in the previous case the hole was identified, with the start and end times given as 15:15 and 16:43 UT. The 32 m ESR observations (Fig. 15) show a depletion at around 15 UT.

The high-latitude convection pattern was inferred from the SuperDARN radars (Fig. 11), with the location of the polar hole observed in the 42 m ESR observations, and GNSS TEC and phase scintillation measurements overlaid as in the previous case study. The 32 m ESR observations (Fig. 9) were directed poleward; indicating that this is a polar hole rather than the ionospheric trough, which would be located equatorward of the radar. A substantial plasma velocity of some 300 m s$^{-1}$ towards the radar was observed at 16:00 UT, indicating cross-polar flow in the equatorward direction. The high-latitude convection pattern inferred from the SuperDARN radars also shows antisunward cross-polar flow, but with a more asymmetric convection pattern than was observed on 17th December 2014. On 10th December 2015 there was a clear dominant dusk cell, drawing plasma across the polar cap from the pre-noon sector. The polar hole observed with the 42 m dish of the ESR was in the sunward return flow in the dusk convection cell.

The phase scintillation plot for 15:16 to 16:14 UT (upper right panel of Fig. 11) has some satellite trajectories passing through the hole boundary, but displays no significant scintillation on any of the paths. The later plot (second panel from the bottom on the right panel of Fig. 11) does contain phase scintillation seen however none of the elevated scintillation matches up to hole boundaries, instead, the scintillation is seen in regions of high and elevated electron density.

## 4 Discussion

A series of polar ionospheric holes have been detected in the high latitude nightside ionosphere in case studies close to winter solstice, under varying solar intensities and geomagnetic disturbance levels. The first study on 17th December 2014 was characterised by high levels of solar activity (198.5 sfu) and quiet geomagnetic conditions. The second case study, on 10th December 2015 also had lower levels of solar activity of (108.5 sfu), but had more active geomagnetic conditions ($K_p$=3) than in the previous study. A third case study, under quiet geophysical conditions ($K_p \leq 2$) and moderate solar activity (F10.7 cm solar flux = 116.7 sfu) on 12th December 2015 showed similar results (not shown).

Ionospheric polar holes contain much lower electron densities than those detected through the rest of the day, this study used the maximum density at a given time dropping 35% below the daily average maximum density to identify these holes. The changes in electron density are associated with large electron density gradients. Table 1 shows the electron density gradients and average hole electron density, based on observations from the ESR 42 m. The average polar hole density observed in this study is comparable to those previously reported of $10^8$-$10^{11}$ electrons·m$^{-3}$ (Obara and Oya, 1989, Benson and Grebowsky, 2001). Steep electron density gradients are observed at the edges of the holes, these are expressed in units of $\Delta N_e \cdot m^{-3} \cdot h^{-1}$. Although these gradients are expressed in units of h$^{-1}$ they were calculated from successive observations by the ESR 42 m (these measurements are typically one minute apart). The spatial extent of these holes was at least several hundred kilometres, as inferred from the GNSS TEC measurements (all studies) and the ESR 32 m observations (case study from 17th December 2014). Polar holes are usually associated with quiet geomagnetic conditions ($K_p<2$). It is notable that, on 10th December 2015, a polar hole was observed under more active geomagnetic conditions ($K_p$=3).

The IMF conditions during the time when the polar holes were observed, and for several hours beforehand, were appropriate for antisunward cross-polar convection. The ground level solar terminator for winter is only above 70° MLAT between 15 UT and slightly after 21 UT, reaching a maximum latitude of just under 76° MLAT on the dayside at around 21 UT, creating the possibility that plasma within the high-latitude convection pattern could circulate in perpetual darkness, thus undergoing recombination whilst simultaneously being insulated from photoionisation, or precipitation, creating a polar hole.

Phase scintillation has previously been observed to coincide with large plasma gradients such as on the edge of ionospheric enhancements such as polar cap patches (Jin et al., 2017), the tongue of ionisation (van der Meeren et al., 2014), plasma structures associated with the aurora (Kinrade et al., 2013; Oksavik et al., 2015; van der Meeren et al., 2015) and the mid-latitude trough (Pryse et al., 1991). The structures that cause scintillation arise due to the Gradient Drift Instability and/or the Kelvin Helmholtz Instability (Keskinen and Ossakow, 1983; Carlson et al., 2008). In the present study, once the boundaries and the large electron density gradients associated with them were identified, these boundaries were investigated for elevated levels of phase scintillation. A threshold of 0.2 rad was used, the purpose of this low value was to ensure that any possible indication of phase scintillation was included. Across all of the observed GNSS points coinciding with the polar hole

boundaries no such levels of phase scintillation were detected. Phase scintillation usually dominates at high latitude (e.g., Prikryl et al., 2015), although amplitude scintillation has also been observed (e.g. Mitchell et al., 2005). The present study focuses upon phase scintillation as no amplitude scintillation, defined as when the S4 index was greater than 0.2, was observed on any of the TEC gradients at the boundaries of the polar holes.

245    This is not the first time a plasma density enhancement has been observed without corresponding phase scintillation. Van der Meeren et al. (2016) observed a Sun-aligned polar cap arc under quiet geomagnetic conditions without corresponding scintillation. In the present study some phase scintillation was observed, however, these points coincide with increases in TEC and the edges of spikes in electron densities at other locations. In the second case study (10$^{th}$ December 2015) phase scintillation was observed at a point associated with elevated TEC (lower right panels of Fig. 11), but this was not associated

250    with the assumed boundary of the polar hole.

   When phase scintillation was observed it was always associated with electron density gradients, but converse is not always true. Therefore it appears that some minimum level of overall electron density is needed for phase scintillation to occur. Given that it is the presence of small scale structures that cause scintillation, this suggests that these small scale structures have not arisen.

255    Figure 12 shows phase scintillation as a function of TEC and TEC rate of change. This figure also includes data from a third study, using data from 12$^{th}$ December 2015, which was consistent with the interpretation presented here, but which has been omitted in the interest of concision. Low scintillation can be seen at all TEC levels and for a majority of the range of TEC rates of change. On the other hand, elevated scintillation levels are only seen above approximately 6 TECU suggesting that a minimum electron density is required. This is not a new idea, in his review paper Aarons (1982) commented 'if the ionosphere

260    is perturbed on a percentage basis, *change in N* in the trough will be small since *N* is low; scintillations will then be low.' The current paper provides observational evidence to support this suggestion that a minimum electron density is required. The current paper is also consistent with suggestions made by Prikryl et al. (2015), where the strongest phase scintillations were found to be highly collocated with regions that are ionospheric signatures of the coupling between the solar wind and magnetosphere. Polar holes appear to be areas of weak coupling, hence less scintillation.

265    In this study the phase scintillation index ($\sigma_\phi$) has been calculated across a 60 second interval, in line with common practice within this field. However, if this index was computed across a shorter time interval, then it is possible that elevated values of $\sigma_\phi$ may be associated with the edge of the polar hole. This would be an interesting topic for a future paper. Further developments upon this work would expand the observations of the polar holes discussed to a larger number of examples under a wider range of geophysical conditions. Polar ionospheric holes could be tracked by making observations with a higher

270    temporal resolution at a large number of regularly spaced locations. The advent of EISCAT-3D (McCrea et al., 2015), which will give unprecedented temporal and spatial coverage, will enable such studies in the European sector of the high-latitude

ionosphere. The ability to observe the evolution of polar holes over time will give a new, deeper, understanding of these features and how they influence practical radio systems such as GNSS.

## 5 Conclusions

275   Polar ionospheric holes are regions of electron density depletions containing large electron density gradients at their boundaries. This paper reports case study observations of polar ionospheric holes conducted using the ESR and GNSS receivers.  These holes were observed during both quiet and moderately disturbed geomagnetic conditions, under a range of solar activities. Steep electron density gradients have been associated with phase scintillation at GNSS frequencies in previous studies, however no enhanced scintillation was detected upon the electron density gradients at these boundaries. Phase

280   scintillation was only observed when electron density levels were elevated above 6 TECU. Aarons (1982) suggested that a minimum density level may be required for scintillation to occur, and the present study provides supporting observational evidence. We conclude that both a minimum electron density level and a sharp gradient in the election density must be present for instability mechanisms to produce scintillation structures.

### Author contribution

285   This work was led by Luke Jenner, under the guidance of Alan Wood. Kjellmar Oksavik provided the GNSS TEC and scintillation data, together with guidance regarding their interpretation. Tim Yeoman and Alexandra Fogg provided the SuperDARN electric potential maps, together with guidance regarding their interpretation. Anthea Coster provided the TEC maps, together with guidance regarding their interpretation. All authors contributed to the discussion. The manuscript was prepared by Luke Jenner and Alan Wood.

### Competing interests

290   The authors declare that they have no conflict of interest.

### Acknowledgements

EISCAT is an international facility supported by the national science councils of China, Finland, Japan, Norway, Sweden, and the United Kingdom. The assistance of Ingemar Häggström and colleagues at the EISCAT Scientific Association in running

295   the experiments is gratefully acknowledged. The data used in this paper is publicly available at https://www.eiscat.se. The assistance of Steve Crothers and Matthew Wild at Rutherford Appleton Laboratory with the data processing is gratefully acknowledged. The GNSS TEC and scintillation data were provided by Kjellmar Oksavik at the University of Bergen, and is supported by the Norwegian Research Council under contracts 212014 and 223252. The authors acknowledge the use of

SuperDARN data, data for which is available at https://vt.superdarn.org. SuperDARN is a collection of radars funded by national scientific funding agencies of Australia, Canada, China, France, Italy, Japan, Norway, South Africa, United Kingdom and the United States of America.' Alexandra Fogg is supported by a studentship from the Science and Technology Facilities Council (UK). The assistance of Nathan Brown with the production of Fig. 5 and Fig. 11 is gratefully acknowledged. GPS TEC data products and access through the Madrigal distributed data system are provided to the community (http://www.openmadrigal.org) by the Massachusetts Institute of Technology (MIT) under support from US National Science Foundation grant AGS-1242204. Data for TEC processing is provided from the following organizations: UNAVCO, Scripps Orbit and Permanent Array Center, Institut Geographique National, France, International GNSS Service, The Crustal Dynamics Data Information System (CDDIS), National Geodetic Survey, Instituto Brasileiro de Geografia e Estatística, RAMSAC CORS of Instituto Geográfico Nacional de la República Argentina, Arecibo Observatory, Low-Latitude Ionospheric Sensor Network (LISN), Topcon Positioning Systems, Inc., Canadian High Arctic Ionospheric Network, Centro di Ricerche Sismologiche, Système d'Observation du Niveau des Eaux Littorales (SONEL), RENAG : REseau NAtional GPS permanent, GeoNet - the official source of geological hazard information for New Zealand, GNSS Reference Networks, Finnish Meteorological Institute, and SWEPOS - Sweden. Access to these data is provided by madrigal network via: http://cedar.openmadrigal.org/.The $K_p$ index and F10.7 cm solar flux were obtained from the UK Solar System Data Centre at Rutherford Appleton Laboratory. These can be accessed at https://www.ukssdc.ac.uk/. The IMF data were provided by N. Ness and obtained from the CDAWeb at https://cdaweb.gsfc.nasa.gov/.

## References

Aarons, J.: Global Morphology of Ionospheric Scintillations, Proceedings of the IEEE, 70, 4, 360-378, doi: 10.1109/PROC.1982.12314, 1982.

Alfonsi, L., Spogli, L., De Franceschi, G., Romano, V., Aquino, M,. Dodson, A., and Mitchell C. N.: Bipolar climatology of GPS ionospheric scintillation at solar minimum, Radio Sci. , 46, RS0D05, doi:10.1029/2010RS004571, 2011.

Anderson, D. N., Buchau, J., and Heelis R. A.: Origin of density enhancements in the winter polar cap ionosphere, Radio Sci., 23, 513-519, doi: 10.1029/RS023i004p00513, 1988.

Benson, R., and Grebowsky, J.: Extremely low ionospheric peak altitudes In the polar hole region, Radio Sci., 36, 277-285, doi:10.1029/1999rs002401, 2001.

Briggs, B.H., and Parkin I. A.: On the variation of radio star and satellite scintillation with zenith angle, J. Amos. Terr. Phys., 25, 339-365, doi:10.1016/0021-9169(63)90150-8, 1963.

Brinton, H., Grebowsky, J., and Brace L.: The high-latitude winter F-region at 300 km: Thermal plasma observations from Ae-C, J. Geophys. Res., 83, 4767-4776, doi:10.1029/Ja083ia10p04767, doi.org/10.1016/0273-1177(91)90317-D, 1978.

Buchau, J. and Reinisch, B. W.: Electron density structures in the polar F region, Adv. Space Res., 11(10), 29-37, 1991.

330 Buchau, J., Reinisch, B. W., Weber, E. J., and Moore, J. G.: Structure and dynamics of the winter polar cap F region, Radio Sci., 18, 995-1010, https://doi.org/10.1029/RS018i006p00995, 1983.

Carlson, H. C., Oksavik, K., Moen, J., van Eyken, A.P., and Guio, P.: ESR mapping of polar-cap patches in the dark cusp, Geophys. Res. Lett., 29 (10), 1386, doi:10.1029/2001GL014087, 2002.

Carlson, H. C., Oksavik, K., Moen, J., and Pedersen, T.: Ionospheric patch formation: Direct measurements of the origin of a
335 polar cap patch, Geophys. Res. Lett., 31, L08806, doi:10.1029/2003GL018166, 2004.

Carlson, H. C., Moen, J., Oksavik, K., Nielsen, C. P., McCrea, I. W., Pedersen, T. R., and Gallop, P.: Direct observations of injection events of subauroral plasma into the polar cap, Geophys. Res. Lett., 33, L05103, doi:10.1029/2005GL025230, 2006.

Carlson, H., Oksavik, K., and Moen, J.: On a new process for cusp irregularity production, Ann. Geophys., 26, 2871-
340 2885, doi:10.5194/angeo-26-2871-2008, 2008.

Cervera, M., and Thomas, R.: Latitudinal and temporal variation of equatorial ionospheric irregularities determined from GPS scintillation observations, Ann. Geophys., 24, 3329-3341, doi:10.5194/Angeo-24-3329-2006, doi: 10.5194/angeo-24-3329-2006, 2006.

Chisham, G., Lester, M., Milan, S. E., Freeman, M. P., Bristow, W. A., Grocott, A., McWilliams, K. A., Ruohoniemi, J. M.,
345 Yeoman, T. K., Dyson, P. L., Greenwald, R. A., Kikuchi, T., Pinnock, M., Rash, J. P. S., Sato, N., Sofko, G. J., Villain, J.-P., and Walker, A. D. M.: A decade of the Super Dual Auroral Radar Network (SuperDARN): Scientific achievements, new techniques and future directions, Surv. Geophys., 28, 33–109, doi:10.1007/s10712- 007-9017-8, 2007.

Cowley, S.W.H. and Lockwood, M.: Excitation and decay of solar-wind driven flows in the magnetosphere-ionosphere system, Ann. Geophys., 10, 103, 1992.

350 Crowley, G.: Critical Review of patches and blobs, in Polar Cap Boundary Phenomena, in: URSI Review of Radio Science 1993-1996, edited by Stone, W. R., published for the International Union of Radio Science, Oxford University Press, 619-648, doi:10.1029/2009JA014985, 1996.

De Franceschi, G., Spogli, L., Alfonsi, L. et al. The ionospheric irregularities climatology over Svalbard from solar cycle 23. Sci Rep 9, 9232 (2019) doi:10.1038/s41598-019-44829-5

355 Elmas, Z., Forte, B. and Aquino, A.: The impact of ionospheric scintillation on the GNSS receiver signal tracking performance and measurement accuracy, URSI General Assembly and Scientific Symposium, doi 10.1109/URSIGASS.2011.6123719, 2011.

Forte B. (2005), Optimum detrending of raw GPS data for scintillation measurements at auroral latitudes, Journal of Atmospheric and Solar-Terrestrial Physics, Vol. 67, N. 12, doi:10.1016/j.jastp.2005.01.011.

360 Forte, B., and Radicella, S.: Problems in data treatment for ionospheric scintillation measurements, Radio Sci., 37, 81-85, doi:10.1029/2001rs002508, 2002.

Foster, J. C.: Ionospheric signatures of magnetospheric convection, J. Geophys. Res., 89, 855-865, 10.1029/JA089iA02p00855, 1984.

Fremouw, E. J., Leadabrand, R. L., Livingston, R. C., Cousins, M. D., Rino, C. L., Fair, B. C., and Long, R. A.: Early results 365 from the DNA wideband satellite experiment—Complex-signal scintillation, Radio Sci., 13, 167–187, doi:10.1029/RS013i001p00167, 1978.

Greenwald, R. A., Baker, K. B., Dudeney, J. R., Pinnock, M., Jones, T. B., Thomas, E. C., Vilain, J. P., Cerisier, J. C., Senior, C., Hanuise, C., Hunsucker, R. D., Sofko, G., Koehler, J., Neilsen, E., Pellinen, R., Walker, A. D. M., Sato, N., and Yamagishi, H.: DARN/SuperDARN: A global view of high latitude convection, Space Sci. Rev., 71, 761-796. doi:10.1007/BF00751350, 370 1995.

Hapgood, M. (2017), Satellite navigation—Amazing technology but insidious risk: Why everyone needs to understand space weather, Space Weather, 15, 545–548, doi:10.1002/2017SW001638.

Jin, Y., Moen, J. I.,. Miloch, W. J., Clausen, L. B. N., and Oksavik, K.: Statistical study of the GNSS phase scintillation associated with two types of auroral blobs, J. Geophys. Res. Space Physics, 121, doi:10.1002/2016JA022613, 2016.

375 Jin, Y., Moen, J., Oksavik, K., Spicher, A., Clausen, L., Miloch, W.: GPS scintillations associated with cusp dynamics and polar cap patches. J. Space Weather Space Clim., 7, A23 doi:10.1051/swsc/2014019, 2017.

Jones, D. G., Walker I. K., and Kersley, L.: Structure of the poleward wall of the trough and the inclination of the geomagnetic field above the EISCAT radar, Ann. Geophys., 15, 740-746, https://doi.org/10.1007/s00585-997-0740-8, 1997.

Kersley, L., Russell, C. D., and Rice, D. L.: Phase scintillation and irregularities in the northern polar ionosphere, Radio Sci.,
380    30, 619, doi:10.1029/94RS03175,1995.

Kersley, L., Jenkins, D. B., and Edwards, K. J.: Nature Phys .Sci., 239, 11, 1972.

Keskinen, M. J. and Ossakow, S. L.: Theories of high-latitude ionospheric irregularities: A review, Radio Sci., 18, 1077-1091,
doi:10.1029/RS018i006p01077, 1983.

Kinrade, J., Mitchell, C. N., Smith, N. D., Ebihara, Y., Weatherwax, A. T., and Bust, G. S.: GPS phase scintillation associated
385    with optical auroral emissions: First statistical results from the geographic South Pole, J. Geophys. Res. Space Physics, 118,
2490–2502, doi:10.1002/jgra.50214, 2013.

Lockwood, M., and Carlson, H. C.: Production of polar cap electron density patches by transient magnetopause reconnection,
Geophys. Res. Lett., 19, 1731 – 1734, 1992.

McCaffrey, A. M., & Jayachandran, P. T. ( 2019). Determination of the refractive contribution to GPS phase "scintillation".
390    Journal of Geophysical Research: Space Physics, 124, 1454– 1469. doi.org/10.1029/2018JA025759

McCrea, I., Aikio, A., Alfonsi, L., Belova, E., Buchert, S., Clilverd, M., Engler, N., Gustavsson, B., Heinselman, C, Kero, J.,
Kosch, M., Lamy, H., Leyser, T., Ogawa, Y., Oksavik, K., Pellinen-Wannberg, A., Pitout, F., Rapp, M., Stanislawska, I., and
Vierinen, J.: The science case for the EISCAT_3D radar, Progress in Earth and Planetary Science, 2:21, doi:10.1186/s40645-
015-0051-8, 2015.

395    Millward, G. H., Moffett, R. J., Balmforth, H. F., and Rodger, A. S.: Modeling the ionospheric effects of ion and electron
precipitation in the cusp, J. Geophys. Res., 104, 24,603, doi.org/10.1029/1999JA900249, 1999.

Mitchell, C. N., Alfonsi, L., De Franceschi, G., Lester, M., Romano, V., and Wernik, A. W.: GPS TEC and scintillation
measurements   from   the   polar   ionosphere   during   the   October   2003   storm,   Geophys.   Res.   Lett.,   32,   L12S03,
doi:10.1029/2004GL021644, 2005.

400    Nishimura, Y., Lyons, L. R., Zou, Y., Oksavik, K., Moen, J. I., Clausen, L. B., Donovan, E. F., Angelopoulos, V., Shiokawa,
K., Ruohoniemi, J. M., Nishitani, N., McWilliams, K. A., and Lester, M.: Day-night coupling by a localized flow channel
visualized by polar cap patch propagation, Geophys. Res. Lett., 41, 3701-3709, doi:10.1002/2014GL060301, 2014.

Nishitani, N., Ruohoniemi, J. M., Lester, M., Baker, J. B. H., Koustov, A. V., Shepherd, S. G., Chisham, G., Hori, T.,
Thomas, E. G., Makarevich, R. A., Marchaudon, A., Ponomarenko, P., Wild, J. A., Milan, S. E., Bristow, W. A., Devlin,

405     J., Miller, E., Greenwald, R. A., Ogawa, T., and Kikuchi, T.: Review of the accomplishments of mid-latitude Super Dual Auroral Radar Network (SuperDARN) HF radars, Prog. Earth Planet. Sci., 6, 27, doi:10.1186/s40645-019-0270-5, 2019.

Obara, T., And Oya, h.: Observations of polar cusp and polar cap ionospheric irregularities and formation of ionospheric holes using topside sounder onboard Exos-C (Ohzora) satellite, Journal of Geomagnetism and Geoelectricity, 41, 1025-1042, doi:10.5636/Jgg.41.1025, 1989.

410     Oksavik, K., Barth, V. L., Moen, J., and Lester, M.: On the entry and transit of high-density plasma across the polar cap, J. Geophys. Res., 115, A12308, doi:10.1029/2010JA015817, 2010.

Oksavik, K., van der Meeren, C., Lorentzen, D. A., Baddeley, L. J., and Moen, J.: Scintillation and loss of lock from poleward moving auroral forms in the cusp ionosphere, J. Geophys. Res. Space Physics, 120, doi:10.1002/2015JA021528, 2015.

Parkinson, M. L., Dyson, P. L., Pinnock, M., Devlin, J. C., Hairston, M. R., Yizengaw, E., and Wilkinson, P. J.: Signatures of

415     the midnight open-closed magnetic field line boundary during balanced dayside and nightside reconnection, Ann. Geophys., 20, 1617-1630, https://doi.org/10.5194/angeo-20-1617-2002, 2002.

Prikryl, P., Jayachandran, P. T., Chadwick, R., and Kelly, T. D.: Climatology of GPS phase scintillation at northern high latitudes for the period from 2008 to 2013, Ann. Geophys., 33, 531-545, doi.org/10.5194/angeo-33-531-2015, 2015.

Pryse, S. E., Wood, A.G., Middleton, H. R., McCrea, I. W., and Lester, M.: Reconfiguration of polar cap plasma in the magnetic

420     midnight sector, Ann. Geophys., 24, 2201-2208, doi.org/10.5194/angeo-24-2201-2006, 2006.

Pryse S. E., Kersley, L., and Russell C. D.: Scintillation near the F layer trough over northern Europe, Radio Science 26, 4, 1105-1114, doi.org/10.1029/91RS00490, 1991.

Rideout, W. and Coster, A. J.: Automated GPS processing for global total electron content data, GPS Solutions, 10, 219-228, doi.org/10.1007/s10291-006-0029-5, 2006.

425     Rino, C. L., Livingston, R. C., Tsunoda, R. T., Robinson, R. M., Vickrey, J. F., Senior, C., Cousins, M. D., Owen, J., and Klobuchar, J. A.: Recent studies of the structure and morphology of auroral-zone F-region irregularities, Radio Sci., 18, 1167-1180, 10.1029/RS018i006p01167, 1983.

Rodger, A. S., Pinnock, M., Dudeney, J. R., Baker, K. B., and Greenwald, R. A.: A new mechanism for polar patch formation, J. Geophys. Res., 99, 6425-6436, doi:10.1029/93JA01501, 1994.

430     Ruohoniemi, J. M., and Greenwald, R. A.: Dependencies of high- latitude plasma convection: Consideration of interplanetary

magnetic field, seasonal, and universal time factors in statistical patterns, J. Geophys. Res., 110, A09204, doi:10.1029/2004JA010815, 2005.

Smith, A. M., Mitchell, C. N., Watson, R. J., Meggs, R. W., Kintner, P. M., Kauristie, K., and Honary, F.: GPS scintillation in the high arctic associated with an auroral arc, Space Weather, 6, S03D01, doi:10.1029/2007SW000349, 2008.

435 Sojka, J., Bowline, M., Schunk, R., Decker, D., Valladares, C., Sheehan, R., Anderson, D., and Heelis, R.: Modeling Polar Cap F-Region Patches Using Time Varying Convection, Geophys. Res. Lett., 20, 1783-1786, Doi:10.1029/93gl01347, 1993.

Spogli, L., Alfonsi, L., De Franceschi, G., Romano, V., Aquino, M. H. O., and Dodson, A.: Climatology of GPS ionospheric scintillations over high and mid-latitude European regions, Ann. Geophys., 27, 3429-3437, doi.org/10.5194/angeo-27-3429-2009, 2009.

440 Thomas, E. G., and Shepherd, S. G.: Statistical patterns of ionospheric convection derived from mid-latitude, high-latitude, and polar SuperDARN HF radar observations, J. Geophys. Res., 123, 3196–3216, doi.org/10.1002/2018JA025280, 2018.

Tsunoda, R. T.: High-latitude F region irregularities: A review and synthesis, Rev. Geophys., 26, 719-760, https://doi.org/10.1029/RG026i004p00719, 1988.

Valladares, C. E., Decker, D. T., Sheehan, R., Anderson, D. N., Bullett, T. and Reinisch, B. W.: Formation of polar cap patches 445 associated with north-to-south transitions of the interplanetary magnetic field, J. Geophys. Res., 103, 14657-14670, https://doi.org/10.1029/97JA03682, 1998.

Valladares, C.E., Basu, S., Buchau, J., and Friis-Christensen, E.: Experimental evidence for the formation and entry of patches into the polar cap, Radio Sci., 29, 167-194, doi: 10.1029/93RS01579, 1994.

van der Meeren, C., Oksavik, K., Lorentzen, D., Moen, J. I., and Romano, V.: GPS scintillation and irregularities at the front 450 of an ionization tongue in the night-side polar ionosphere, J. Geophys. Res. Space Physics, 119, 8624–8636, doi:10.1002/2014JA020114, 2014.

van der Meeren, C., Oksavik, K., Lorentzen, D. A., Rietveld, M. T., and Clausen, L. B. N.:, Severe and localized GNSS scintillation at the poleward edge of the nightside auroral oval during intense substorm aurora, J. Geophys. Res. Space Physics, 120, 10,607–10,621, doi:10.1002/2015JA021819, 2015.

455 van der Meeren, C., Oksavik, K., Lorentzen, D. A., Paxton, L. J., and Clausen, L. B. N.: Scintillation and irregularities from the nightside part of a Sun-aligned polar cap arc, J. Geophys. Res. Space Physics, 121, 5723–5736, doi:10.1002/2016JA022708, 2016.

Vierinen, J., Coster, A. J., Rideout, W. C., Erickson, P. J., and Norberg, J.: Statistical framework for estimating GNSS bias, Atmos. Meas. Tech. Discuss., 8, 9373–9398, doi:10.5194/amtd-8-9373-2015, 2015.

460 Wang, Y., Zhang, Q.‐H., Jayachandran, P. T., Moen, J., Xing, Z.‐Y., Chadwick, R., et al. ( 2018). Experimental evidence on the dependence of the standard GPS phase scintillation index on the ionospheric plasma drift around noon sector of the polar ionosphere. Journal of Geophysical Research: Space Physics, 123, 2370–2378. doi.org/10.1002/2017JA024805

Wannberg, G., Wolf, I., Vanhainen, L.-G., Koskenniemi, K., Röttger, J., Postila, M., Markkanen, J. Jacobsen, R., Stenberg, A., Larsen, R., Eliassen, S., Heck, S., and Huuskonen, A.: The EISCAT Svalbard radar: A case study in modern incoherent 465 scatter radar system design, Radio Sci., 32, 2283–2308, doi:10.1029/97RS01803, 1997.

Walker, I. K., Moen, J., Kersley, L., and Lorentzen, D. A.: On the possible role of cusp/cleft precipitation in the formation of polar-cap patches, Ann. Geophys., 17, 1298-1305, doi.org/10.1007/s00585-999-1298-4, 1999.

Weber, E., Buchau, J., Moore, J., Sharber, J., Livingston, R., Winningham, J., and Reinisch, B.: F-layer ionization patches in the polar cap, J. Geophys. Res., 89, 1683, doi:10.1029/Ja089ia03p01683, 1984

470 Zwickl, R. D., Doggett, K.A., Sahm, S., Barrett, W.P., Grubb, R.N., Detman, T.R., Raben, V.J., Smith, C.W., Riley, P., Gold, R.E., Mewaldt, R.A., Maruyama T.: The NOAA Real-Time Solar-Wind (RTSW) system using ACE data, Space Sci. Rev., 86, 633–648, doi:10.1023/ A:1005044300738, 1998.
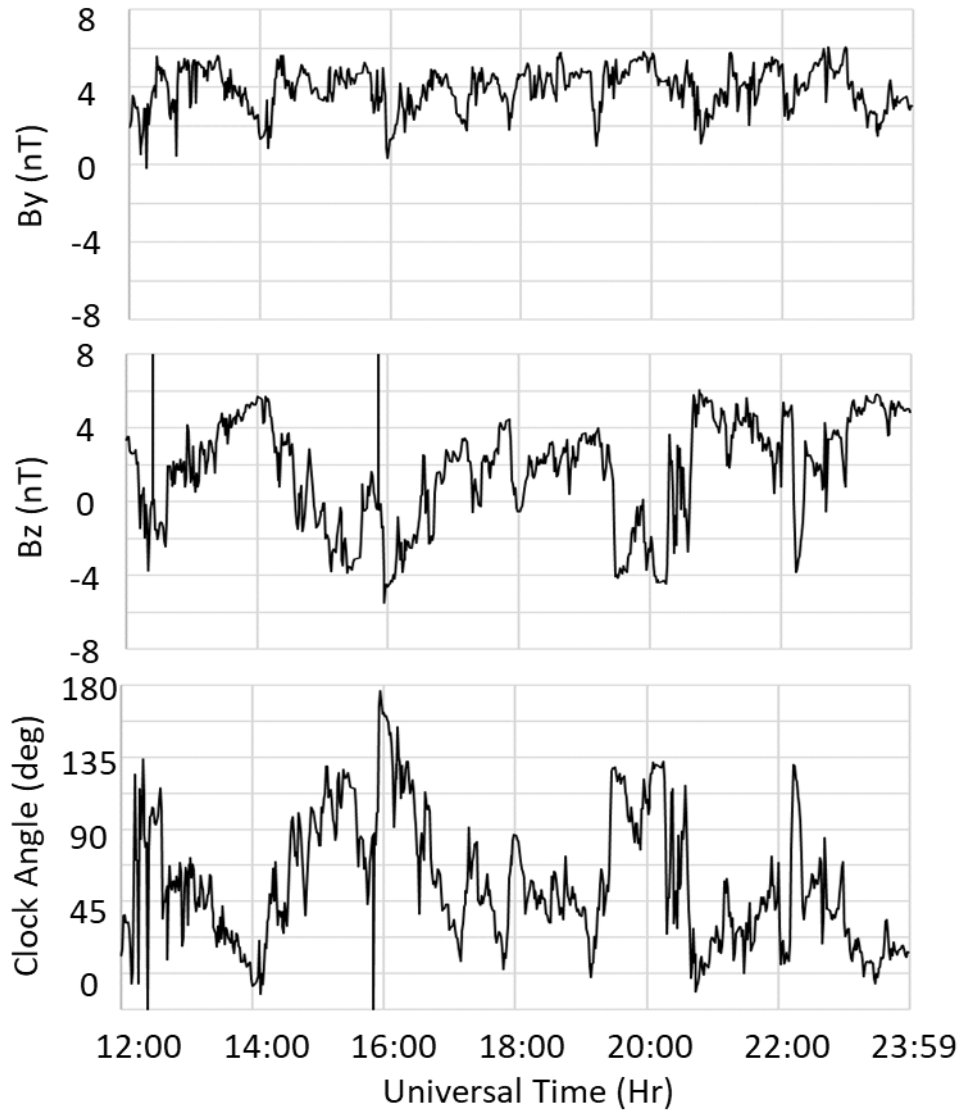
475    **Fig. 1. The y- and z-components of the IMF, and the clock angle observed by the ACE spacecraft between 12:00 UT and 23:59 UT on 17th December 2014. The data have been time shifted to the nose of the Earth's bow shock.**
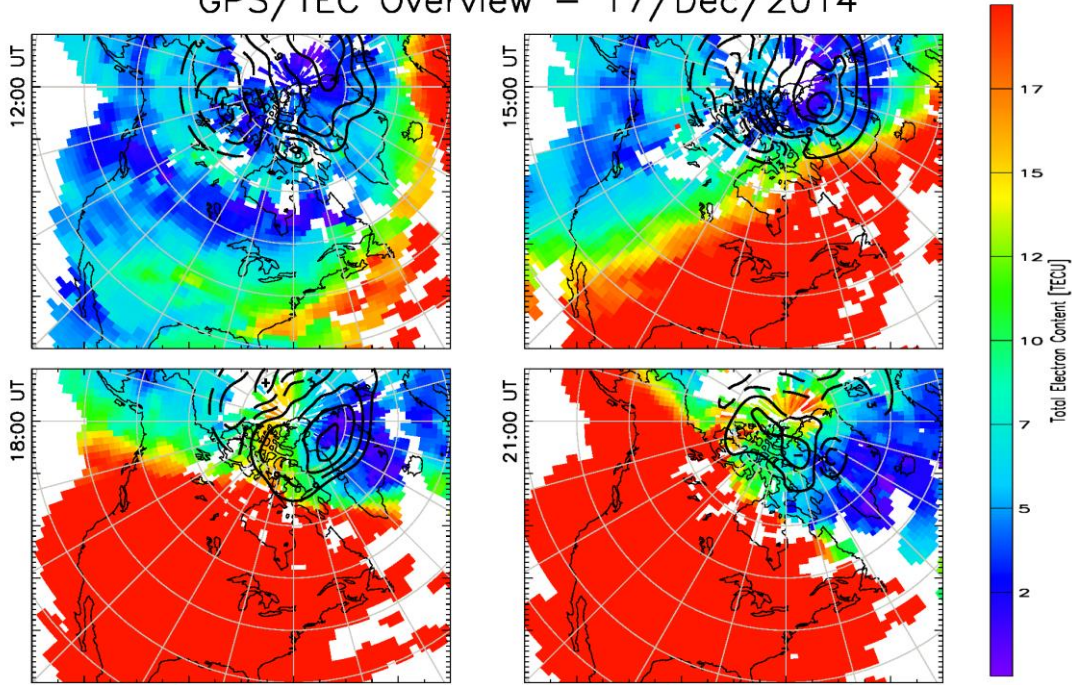
**Fig. 2. TEC maps for the 17th December 2014 extrapolated from TEC collected by a network of GNSS receivers at three hourly intervals between 12 UT and 21 UT.**

480
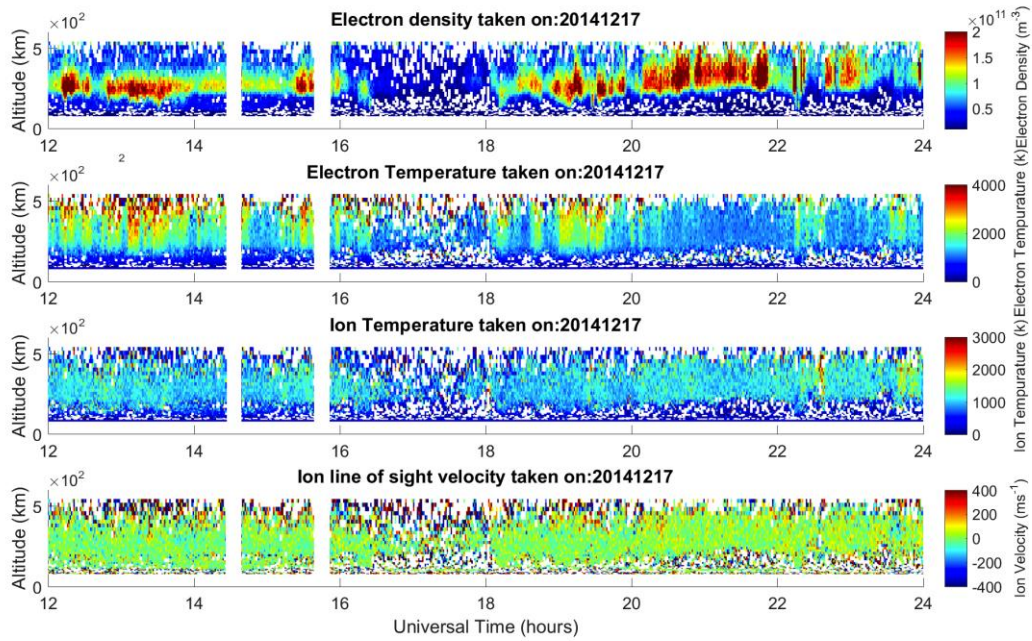
**Fig. 3. Electron densities, electron temperatures, ion temperatures, and ion drift line of sight velocity measured by the 42 m dish of the ESR observing at an azimuth of 184.5° and an elevation of 81.6° between 12:00 UT and 23:59 UT on 17th December 2014.**
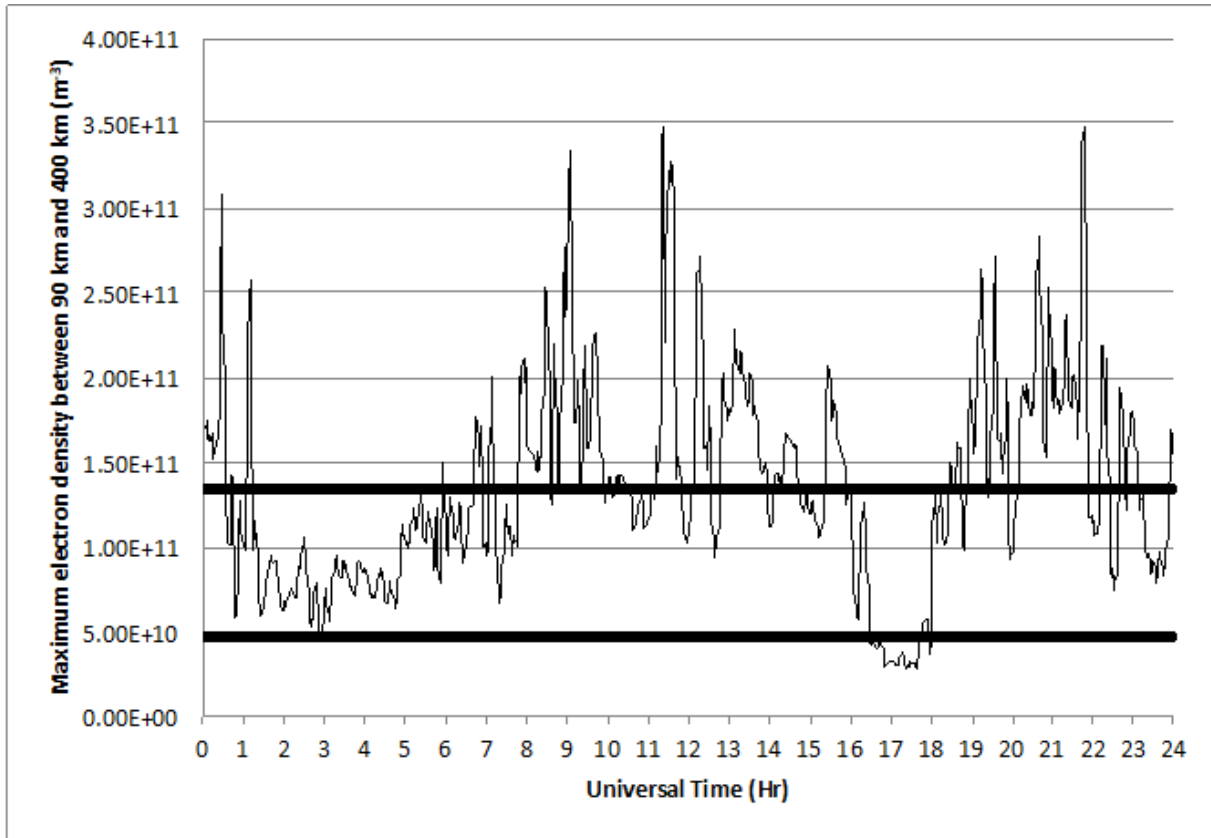
**Fig. 4. Maximum electron density between 90 and 400 km for ESR 42 m observation on the 17th December 2014 at one minute resolution. A five point running mean was applied to these data. The upper horizontal line is the average value and the lower horizontal line is 35% of the average. A hole can be seen between 16:29 and 18:00 UT.**

485
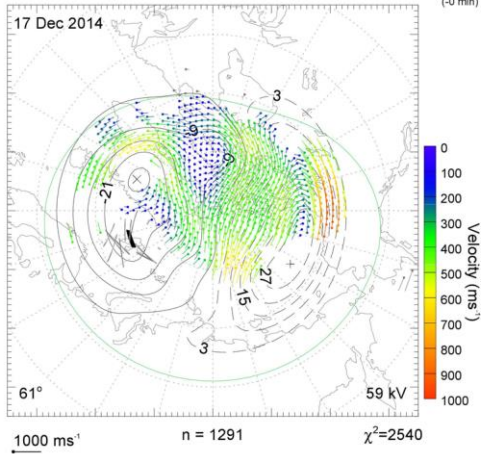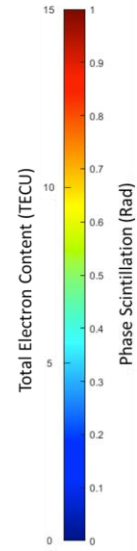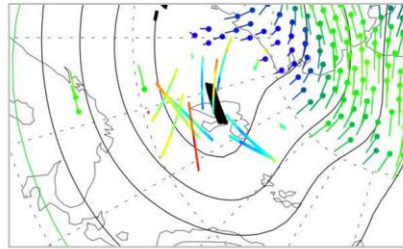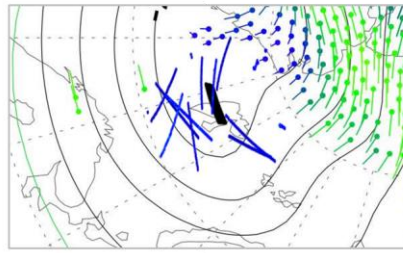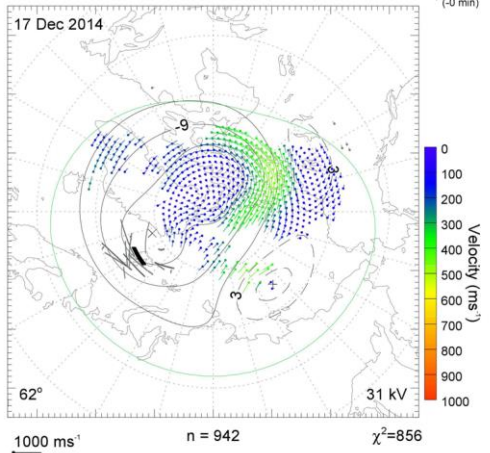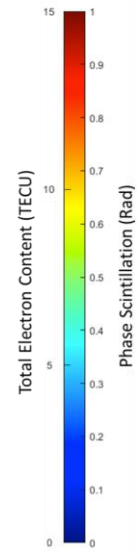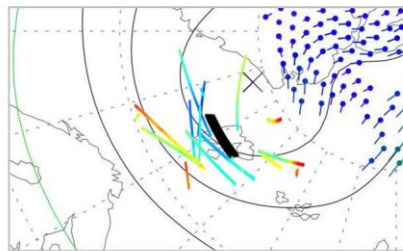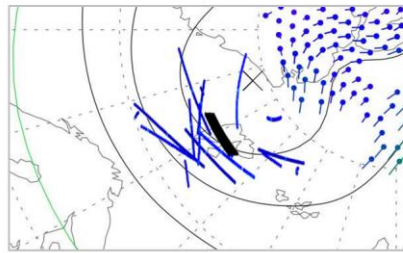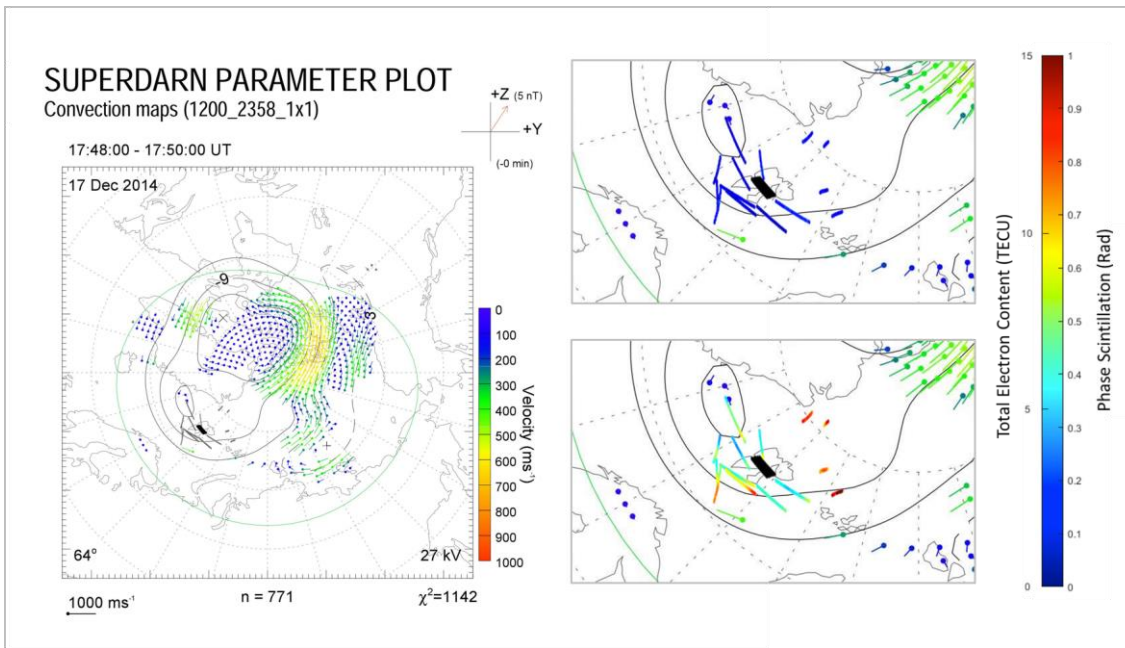
**Fig. 5. Electric potential patterns inferred from the SuperDARN radars for 16:28 UT, 17:14 UT, and 17:48 UT on 17th December 2014 as a function of geomagnetic latitude and magnetic local time. Magnetic noon is at the top of each plot with dusk and dawn on the left- and right- hand sides respectively. Magnetic latitude is indicated by the grey dashed circular lines in 10.0∘ increments. The grey lines show the location of satellite passes from GNSS satellites, assuming an ionospheric intersection of 350 km. The SuperDARN plot from 16:28 UT includes satellite passes from 16:00-16:58 UT, the 17:14 UT plot includes satellite passes from 16:58-17:28 UT, and the 17:48 UT plot includes satellite passes from 17:28-18:02 UT. These time intervals were chosen as inspection of the whole SuperDARN data set at two minute resolution indicated that the convection patterns were relatively stable during these intervals. The right hand side of the panels show the area around the satellite passes in more detail. The multi-coloured colours represent phase scintillation (upper panel in each pair) and TEC (lower panel in each pair). The thick black line indicates the position**
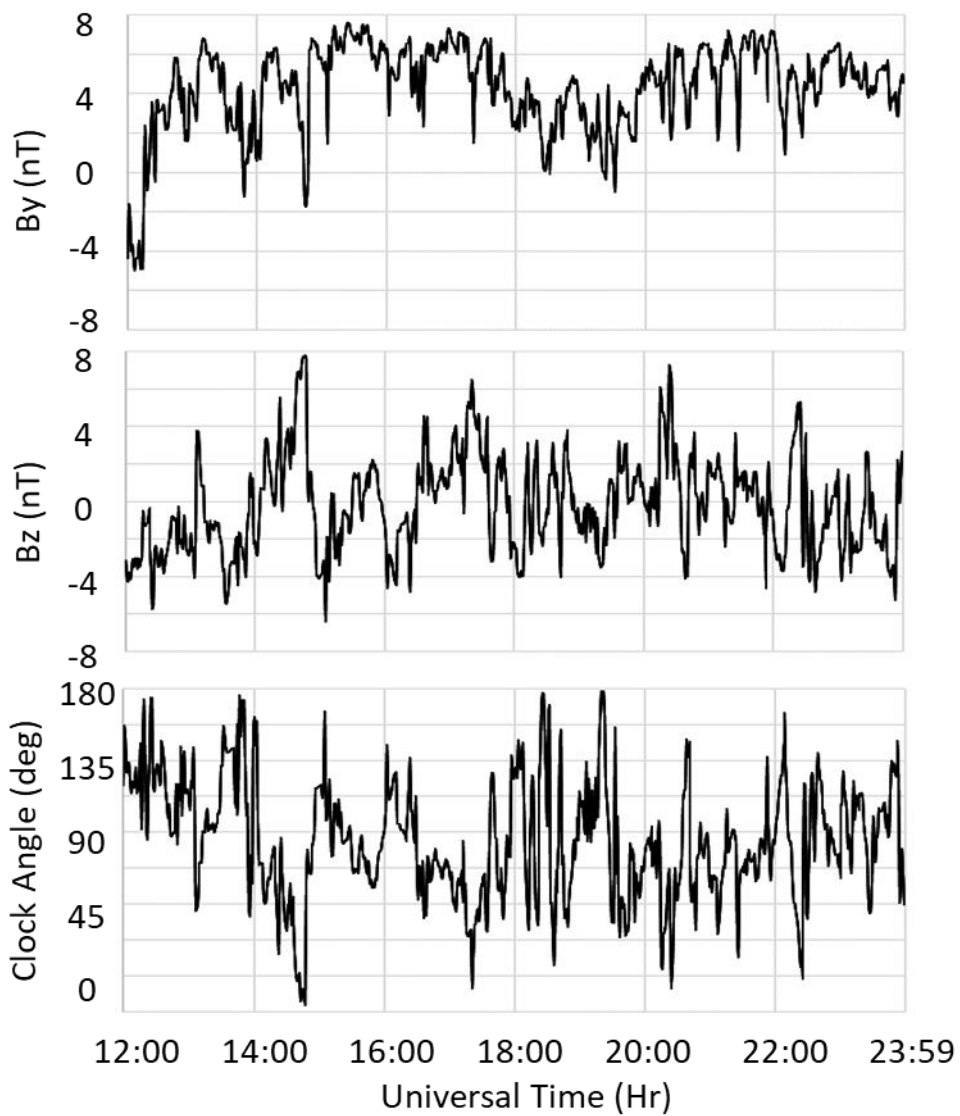
500

Fig. 6. The y- and z-components of the IMF, and the clock angle observed by the ACE spacecraft between 12:00 and 23:59 UT on 10th December 2015, in the same format as Fig. 1. The data have been time shifted to the nose of the Earth's bow shock.
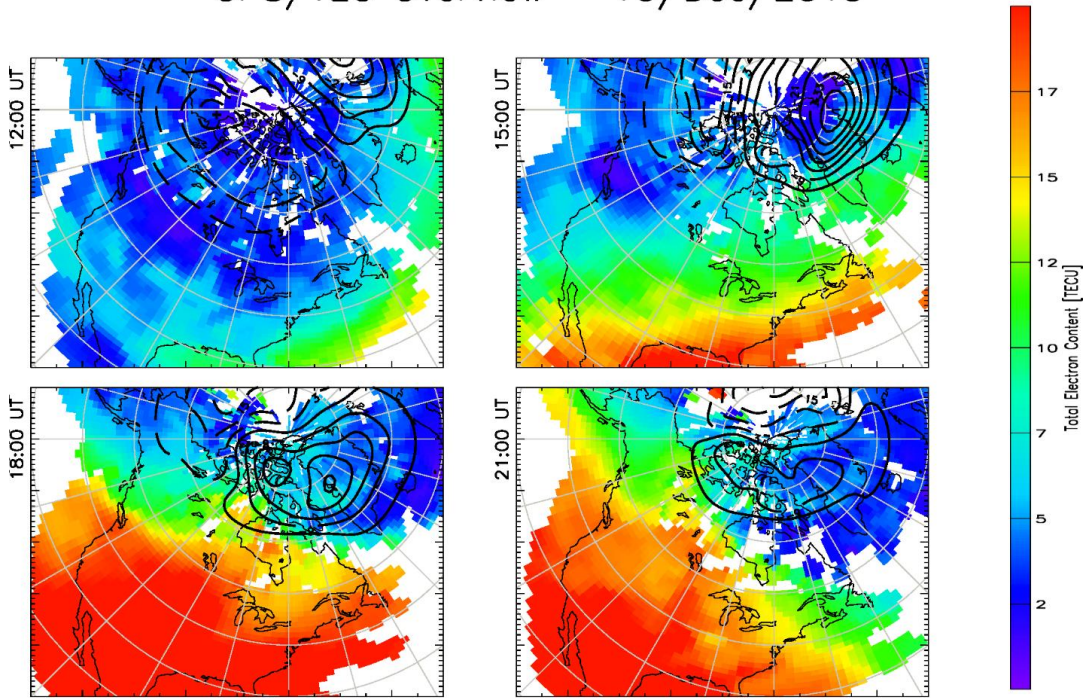
**Fig. 7. TEC maps for the 10th December 2015 extrapolated from TEC collected by a network of GNSS receivers at three hourly intervals between 12 and 21 UT.**
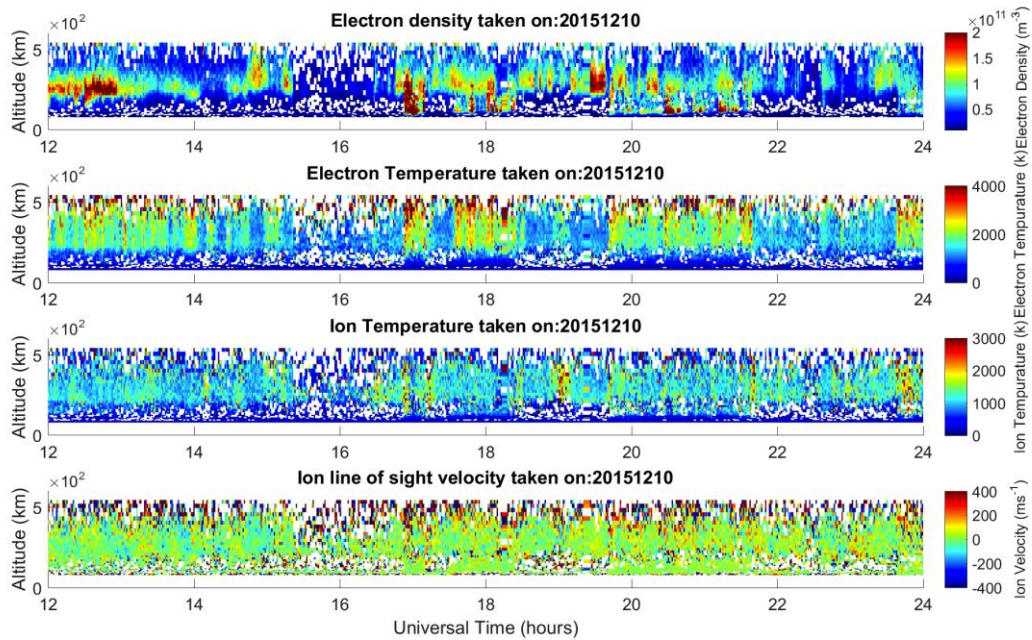
**Fig. 8. Electron densities, electron temperatures, ion temperatures, and ion drift line of sight velocity measured by the 42 m dish of the ESR observing at an azimuth of 184.5° and an elevation of 81.6° between 12:00 and 23:59 UT on 10th December 2015.**
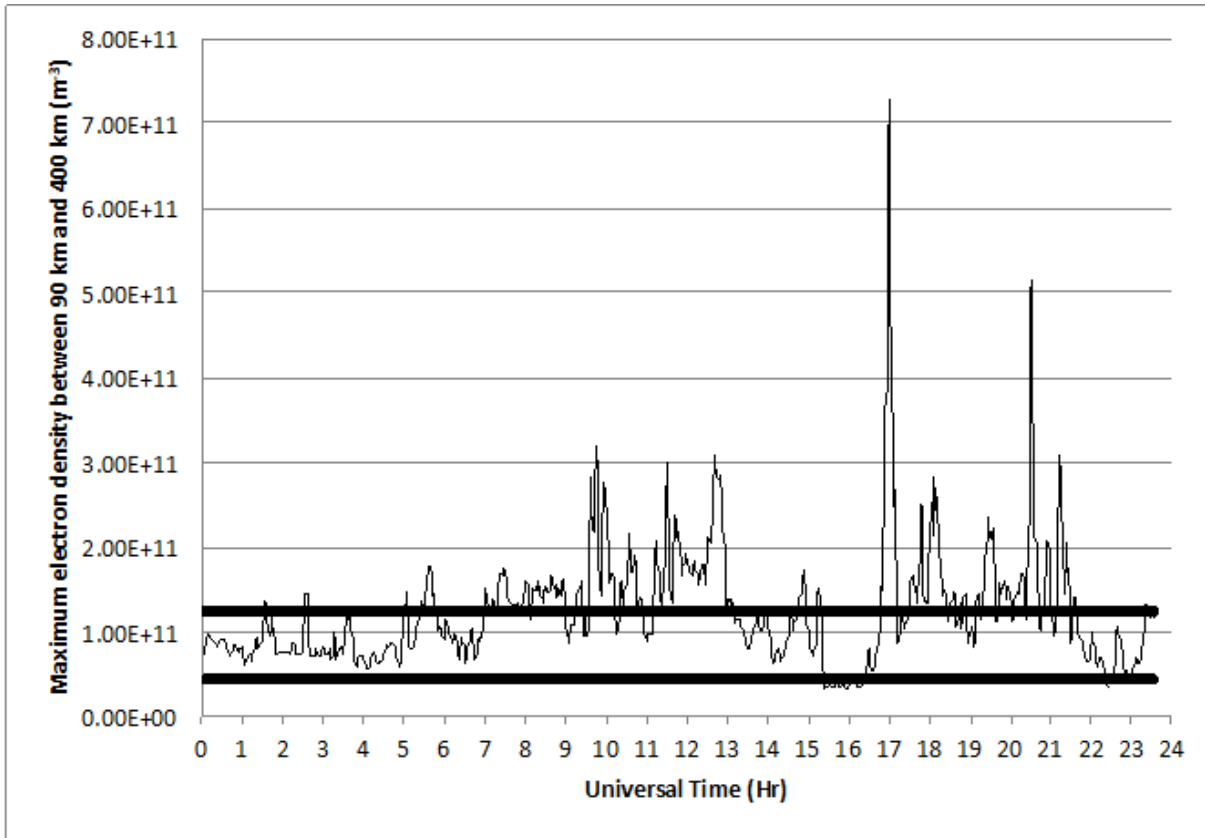
510    **Fig. 9. As Fig. 4 but for 10th December 2015. A polar hole can be seen between 15:24 and 16:25 UT.**
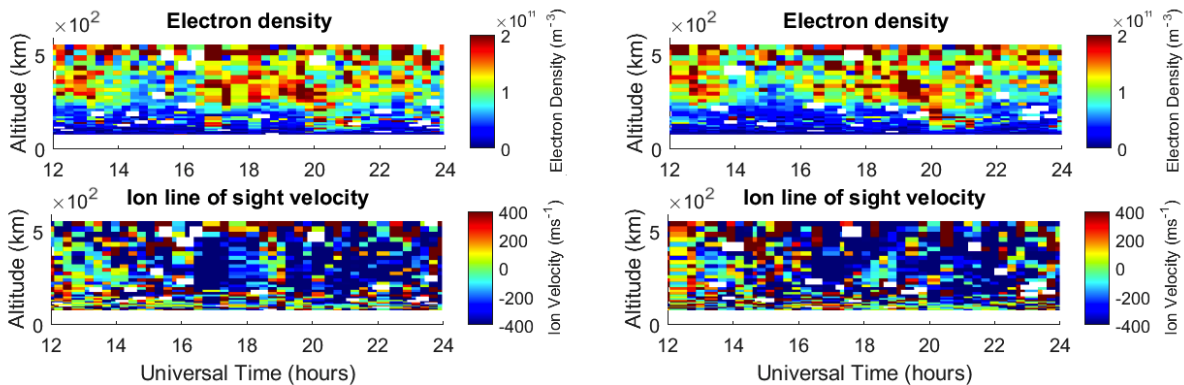
**Fig. 10. Electron densities and ion drift line of sight velocities observed by the 32 m dish of the ESR at -43° azimuth and 30° elevation (left hand side) and at -14° azimuth and 30° elevation (right hand side) between 12:00 and 23:59 UT on 10th December 2015.**
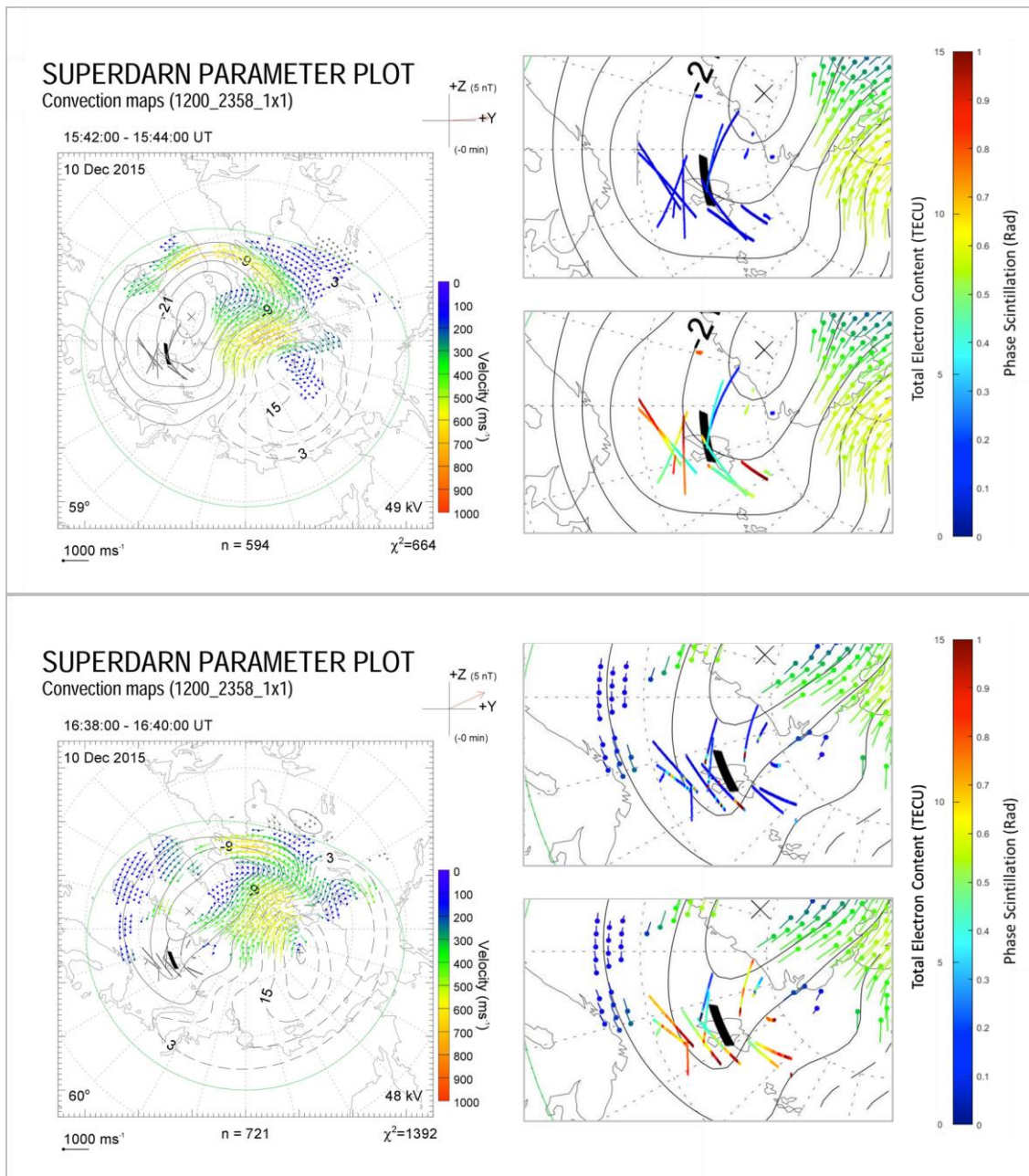
**Fig. 11. Electric potential patterns inferred from the SuperDARN radars for 15:42 UT and 16:38 UT on 10th December 2015, with data from GNSS satellites overlaid in the same format as Fig. 5. The intervals for which the satellite passes were plotted are from 15:16-16:14 UT (15:42 UT plot) and from 16:14-17:04 UT (16:38 UT plot).**

| Date | 1st Edge $\Delta N_e \cdot m^{-3} \cdot h^{-1}$ | 2nd Edge $\Delta N_e \cdot m^{-3} \cdot h^{-1}$ | Average Hole $N_e \cdot m^{-3}$ |
|---|---|---|---|
| 17/12/2014 | 1.0E+11 | 0.91E+11 | 0.40E+11 |
| 10/12/2015 | 3.5E+11 | 1.6E+11 | 0.22E+11 |
| 12/12/2015 | 0.79E+11 | 1.0E+11 | 0.18E+11 |

**Table 1 – The electron density gradient at each edge of the polar hole and the average electron density inside the hole at 350 km observed by ESR 42 m.**

520
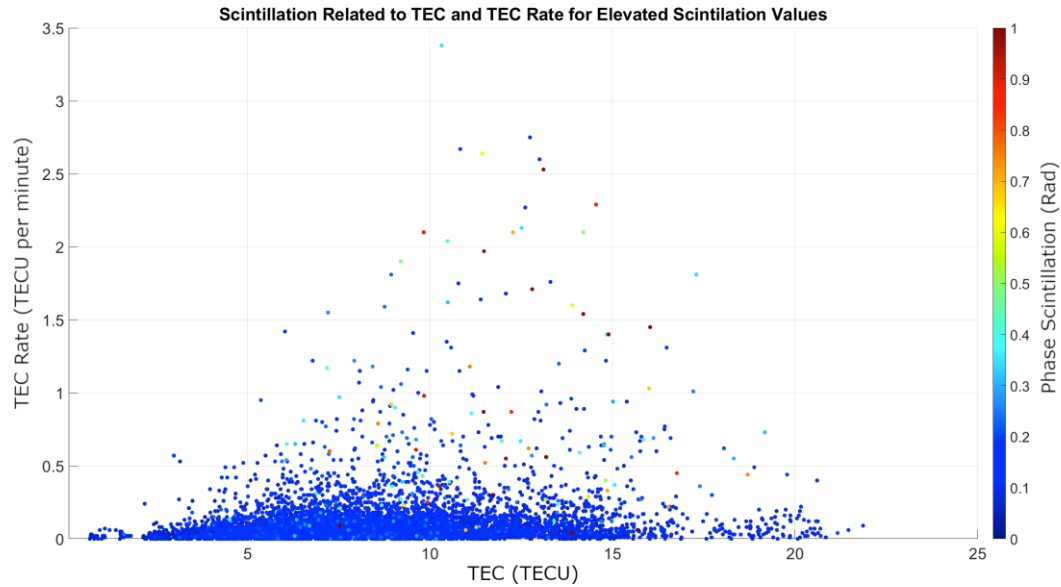
**Fig. 12 – Phase scintillation as a function of TEC and the TEC rate of change per minute for 17th December 2014, 12th December 2015 and 10th December 2015.**